Journal of Radioanalytical and Nuclear Chemistry (2018) 317:307–313
https://doi.org/10.1007/s10967-018-5880-7

Determination of boron and hydrogen in materials for multicrystalline solar cell production with prompt gamma activation analysis

Christian Stieghorst[1,2] · Gabriele Hampel[2] · Barbara Karches[2] · Patricia Krenckel[3] · Petra Kudějová[1] · Christian Plonka[2] · Zsolt Révay[1] · Stephan Riepe[3] · Katharina Welter[2] · Norbert Wiehl[2]

Received: 25 January 2018 / Published online: 27 April 2018

Abstract
For the optimization of the manufacturing process of multicrystalline silicon (mc-Si) for solar cells in order to reduce energy consumption and costs, it is important to know the distribution of the impurities. In our project, we analyzed the raw materials, the crucibles, and the solidified blocks (ingots) with different methods based on neutron activation. In this paper, we present the technique and the results of the boron and hydrogen determination with prompt gamma activation analysis (PGAA). We show that the distribution of boron in the ingots can be successfully described with a Scheil curve. Concerning the raw material, the most relevant information is the average elemental mass fraction. For this purpose, PGAA is well suited since it provides a bulk analysis with detection limits down to the low ng/g range for boron and µg/g range for hydrogen. In this context, the hydrogen content of fluidized bed reactor (FBR) feedstock is discussed in detail. These were the first extensive PGAA studies of the boron and hydrogen content in mc-Si.

Keywords Prompt gamma activation analysis · Multicrystalline silicon · Boron distribution · Hydrogen analysis · Solar cells

Introduction

Mc-Si is an important material for solar cell production. The manufacturing process of mc-Si for solar cells is based on directional solidification in which the molten silicon crystallizes from the bottom to the top of the crucible. The solidification takes place in a *vertical gradient freeze* (VGF) furnace initiated by crystallization seeds and heat extraction at the bottom of the crucible—a brief description of this method can be found, e.g. in Ref. [1]. The result is a solidified block (ingot) of mc-Si. This material is one of the most important materials for commercial solar cells—with special regards to its favorable price-to-performance ratio. Further efforts are being made to reduce the energy consumption and the costs of its manufacturing. In this context, it is important to get reliable information on the content of impurities in the raw materials, the crucibles, and the coatings, as well as their final distribution in the ingot. These data help to understand the behavior of impurities in mc-Si and can be used to validate simulation models.

In our project, we analyzed various materials with different neutron activation techniques and were able to determine the most of the relevant trace elements in silicon. The use of neutron activation techniques is advantageous because of the low detection limits, the straightforward sample preparation—chemical treatment is not necessary—and the negligible matrix dependence. This paper focuses on the determination of boron and hydrogen. While boron is the most important dopant for p-type mc-Si cells, hydrogen is an undesirable impurity. The hydrogen content is of special interest in feedstock materials, because higher hydrogen mass fractions can affect the crystallization

✉ Christian Stieghorst
christian.stieghorst@frm2.tum.de

[1] Heinz Maier-Leibnitz Zentrum (MLZ), Technische Universität München, Lichtenbergstr. 1, 85748 Garching, Germany

[2] Institute of Nuclear Chemistry, Johannes Gutenberg University Mainz, Fritz-Straßmann-Weg 2, 55128 Mainz, Germany

[3] Fraunhofer Institute for Solar Energy Systems (ISE), Heidenhofstraße 2, Freiburg, Germany

process—so that the materials of the ingot and the crucible have a higher tendency to stick together. In the worst case, the crucible may break, and leaking liquid silicon may cause damages inside the VGF furnace. Another problem arising from the presence of hydrogen is the mechanical resilience of mc-Si which decreases with the increasing hydrogen mass fraction [2]. Hydrogen and boron were both measured with prompt gamma activation analysis (PGAA). Additionally, chlorine was analyzed with instrumental neutron activation analysis (INAA) in fluidized bed reactor (FBR) feedstock material, because it is present in the trichlorosilane gas which is used in the production process and may therefore be used for an indirect hydrogen analysis.

The results of the other relevant impurities in mc-Si can be found in earlier publications in the framework of this project—3d transition metals (e.g. cobalt and iron) analyzed with instrumental neutron activation analysis (INAA) are published in [3, 4] and related simulations in [5]. A new approach to determine the n-type dopant phosphorous in solar silicon with a beta-gamma anti-coincidence setup is described in detail in [6]. Additional descriptions of the project and its results can be also found in [7] and [8].

Sample preparation

One of the main advantages of neutron activation analytical techniques is the simple sample preparation. Pieces of crucible materials, granulates of raw materials (feedstock) and coating powders require no further treatment and were just sealed in a bag made of polytetrafluoroethylene (PTFE). In order to analyze the boron distribution in the ingot, the block was cut vertically and horizontally using a band saw (Fig. 1) to a size of approximately $16 \times 11 \times 4$ mm^3 with a mass of 1.6 g. Due to the fact that boron is not a main component of the saw blade and that boron has relatively low mobility in solid silicon, the boron analysis is much less sensitive to the contamination during sawing than the analysis of 3d transition metals. The problems concerning the impurities with a high mobility are described in [3, 4]. Nevertheless, possible surface contaminations of the samples (at least 1 µm) were removed by etching with a mixture of 50% hydrofluoric acid, 70% nitric acid and 100% acetic acid in a ratio of 1:6:2. After etching, the samples were rinsed with Millipore water and analytical grade isopropyl alcohol.

Prompt gamma activation analysis at MLZ

PGAA is based on neutron capture in atomic nuclei. The subsequently formed excited compound nuclei emit energy in the form of element isotope specific prompt gamma rays which can be detected by high-purity germanium detectors (HPGe). As a consequence of the prompt emission of the gamma rays, the irradiation and the measurement have to be performed simultaneously. The detection limits reach down to µg or even ng for several elements. Amongst those elements with low detection limits, boron and hydrogen are particularly interesting for the solar cell production.

The PGAA facility at the MLZ in Garching uses neutrons from the cold source of the reactor. The maximum neutron flux at the sample position is 5×10^{10} cm^{-2} s^{-1} thermal equivalent (focussed) and 2×10^{9} cm^{-2} s^{-1} thermal equivalent (collimated) with an average neutron energy of 1.83 meV (6.7 Å). Smaller samples can be irradiated as a whole—the sample size is up to 2×3 cm^2 under 45°. Two HPGe detectors are arranged perpendicularly to the beam direction. The main detector has a 60%

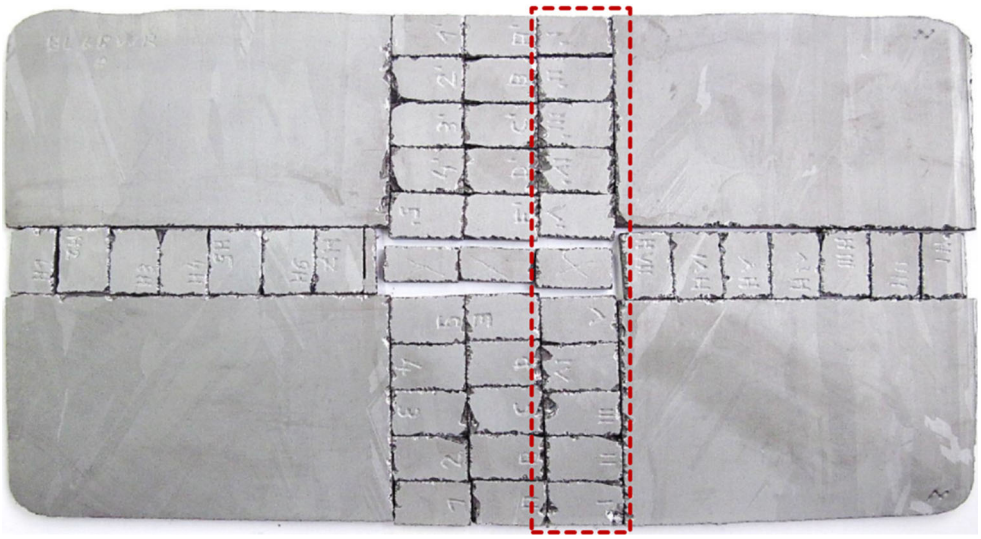

Fig. 1 Samples of a mc-Si block after band sawing: The picture shows a vertical cross section of the ingot with a vertical and a horizontal sample dissection. The marked samples with the Roman letters were analyzed by PGAA

relative efficiency and is surrounded by a bismuth germanate $Bi_4Ge_3O_9$ (BGO) scintillator for Compton suppression. Detailed information on the technical properties can be found in [9].

PGAA provides average mass fractions in the sample (bulk analysis). This is the information needed for the raw materials like feedstock silicon.

Boron and hydrogen analysis

Any interfering signals from the sample environment have to be reduced to the minimum. Therefore, the samples were fixed in a wide web of high-purity fluorinated ethylene propylene (FEP) copolymer strings with a diameter of 0.28 mm. This approach has been used successfully for various measurements at the PGAA instrument [10]. The negligible amount of hydrogen in the sample holder kept the neutron scattering at minimum and provided a low gamma background. For the same reason, all measurements were performed under vacuum (< 0.3 mbar). The measurement time ranged from half an hour to 8 h, mainly depending on the mass fraction of the trace elements and the sample mass.

The spectra were analyzed using the Hypermet-PC software [11]. As a consequence of the kinetics of the $^{10}B(n,\alpha\gamma)^7Li$ reaction, the shape of the boron peak differs from the most of the other gamma lines arising from (n,γ) reactions—it is Doppler-broadened due to the random angular distribution of the reaction products and the release of the gamma quanta from the excited ^7Li during the flight ($T_{1/2}$ = (73 ± 2) fs [12]). The reaction can be written as follows [13]:

$$^{10}\mathrm{B} + \mathrm{n} \rightarrow \left[^{11}\mathrm{B}\right]^{*} \rightarrow \begin{cases} \alpha + {}^{7}\mathrm{Li}^{*} \rightarrow \alpha + {}^{7}\mathrm{Li} + \gamma + 2.31\ \mathrm{MeV}\ (93.7\%) \\ \alpha + {}^{7}\mathrm{Li} + 2.79\ \mathrm{MeV}\ (6.3\%) \end{cases}. \quad (1)$$

The broadened peak shape was calculated with a Gnuplot script based on the method of *Magara* and *Yonezawa* described in [14] and led to an accurate fit for boron mass fraction in the ng/g and low-µg/g range (see example in Fig. 2). The shape of the boron peak depends on the stopping power in the sample material and higher boron mass fractions can complicate the fitting procedure with this approach (see remarks in [15] and [16]). The peak areas of the samples with high boron mass fractions $c_B \gg 1$ µg/g were calculated using peak summing after linear background subtraction, since in this case the peak-to-Compton ratios were high, and thus fitting the background with a step function gave no significant advantage.

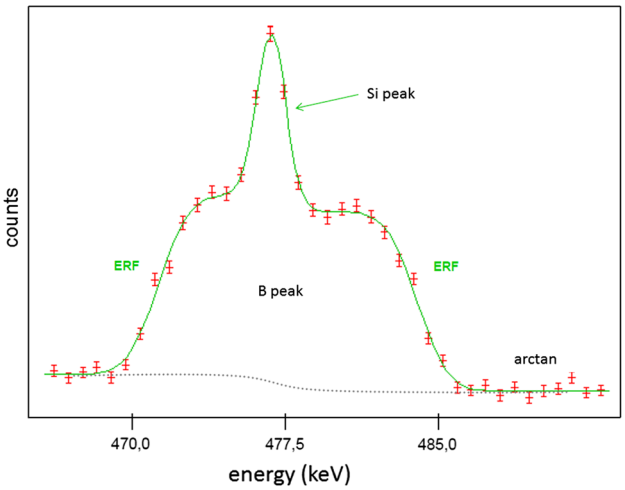

Fig. 2 Fitting of the Doppler-broadened boron peak according to [14]. Two error functions (ERF) are used to fit both sides of the boron peak, while a Gaussian fits the silicon peak. The background is approximated with an arctangent as a step function (drawn schematically)

Nevertheless, other fitting approaches are also equally feasible [17–19].

Mass fractions, uncertainties and detection limits

The final steps of the activation analysis are calculating the mass fractions ("concentrations"), the uncertainties, and the detection limits of the elements. The values are indicated in µg/g or ng/g in accordance with the SI. This is equal to the units ppm_w and ppb_w which are commonly used in solar silicon research. To eliminate the possible effects during the irradiation, such as fluctuations of the neutron flux, inhomogeneity of the beam profile and neutron self-shielding, it is advantageous to use an internal standard. This is usually a main component of the sample in the form of a compound with a defined stoichiometric proportion or in the form of an element. The internal standard I is exposed to the same effects as the interesting trace elements. In our case, silicon can be used as an internal standard (for the crucibles SiO_2 or Si_3N_4).

Silicon, boron, and hydrogen show a regular behavior concerning the neutron capture cross sections, also in the energy region of cold neutrons. The calculation of the trace element content $\rho_{x/i}$ can be done by the following expression [20]:

$$\rho_{x/I} = \frac{N_{x,\gamma} M_x}{\varepsilon_{x,\gamma}\sigma_{x,\gamma}} \Big/ \frac{N_{i,\gamma} M_i}{\varepsilon_{i,\gamma}\sigma_{i,\gamma}}. \quad (2)$$

Hereby N is the net peak area, M the relative atomic mass, ε the counting efficiency and σ is the partial gamma-ray

production cross section. The indices x and i stand for the trace element (in our case hydrogen or boron) respective the internal standard (silicon) and γ for a given gamma-ray. In the analyzed samples, the proportion of the internal standard is almost 100%, so that $\rho_{x/I}$ is a good approximation for the mass fraction c_x.

Background correction was necessary for both hydrogen and boron. To take neutron scattering in the sample into account, a piece of n-type silicon of the same size as the sample was chosen for the background determination. In an analogous matter, another blank with a similar geometry to the feedstock granulate was chosen for hydrogen analysis. Neutron self-shielding and gamma-ray self-absorption had only negligible influence on the results, due to the low cross section of silicon $\sigma_{th} = 0.166$b in combination with the small thickness of the samples $d_{max} = 4$ mm and due to sufficient homogeneity within the sample. This was also confirmed by repeated measurements of the same sample in different orientations.

If not mentioned separately, the uncertainties are combined standard uncertainties. The calculation of the detection limits and the decision thresholds is derived from the international norm ISO 11929 based on the Bayesian approach. For the detection limit of boron in silicon a minimum of 17 ng/g and for hydrogen 1 µg/g could be reached.

Results of the boron analysis

Vertical boron distribution

On the one hand, boron is the most important dopant for p-type Si, but on the other hand, it is an undesirable impurity in n-type Si. In both cases, the information on the initial boron mass fraction in the raw material is necessary to predict the distribution in the final product.

In the following section, we discuss the boron distribution of a p-type ingot (size 220 × 220 × 120 mm^3) and an alternately doped ingot ("zebra"-ingot). The vertical cut of the p-type ingot shows a perfect Scheil curve which can be described by the following equation [21]:

$$c_S = kc_0(1-f_S)^{k-1}. \quad (3)$$

Hereby c_S is the mass fraction in the solidified phase as a function of the relative ingot height. The parameter k is the segregation coefficient which describes the ratio of the mass fraction in the solid phase to that in the liquid phase. The product of k and initial mass fraction c_0 is the mass fraction at the starting point of the solidification at the bottom of the crucible and f_S is the already solidified fraction. The parameters emerging from the fit in (Fig. 3) are $c_0 = (154 \pm 1.5)$ ng/g and $k = 0.791 \pm 0.009$. The

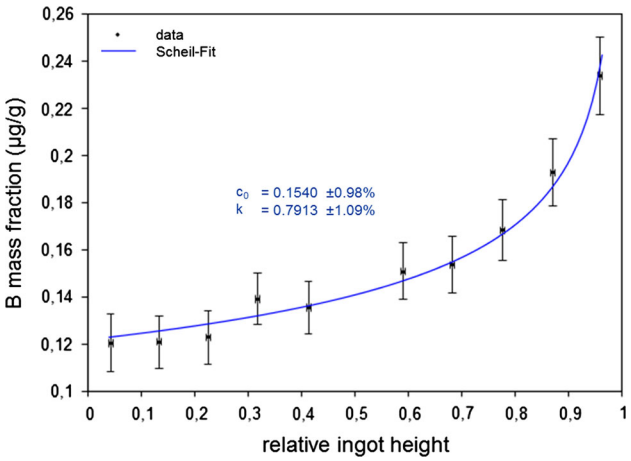

Fig. 3 The boron mass fraction as a function of the relative height of the p-type ingot (Scheil fit)

plotted initial mass fraction c_0 is in good agreement with the measurement of the raw material—an *upgraded metallurgical grade* (UMG) feedstock—that shows a boron mass fraction of (153 ± 11) µg/g. The plotted segregation coefficient conforms to the value taken from the literature $k = 0.8$ [22]. This validates that the Scheil equation can be used to describe the boron distribution in mc-Si produced by directional solidification.

A more complex doping profile was investigated for the so-called "zebra"-ingot in which boron and phosphorus were alternately added during the crystallization. This ingot was produced for testing different methodological approaches during the solidification process at the ISE and was finally used to test if the measurements are in accordance with the planned dopant distribution. The PGAA results of the boron distribution show a good agreement with the predicted doping profile (Fig. 4). The deviation in the lower part of the ingot can be explained by a difference from the original plan at the beginning of the production

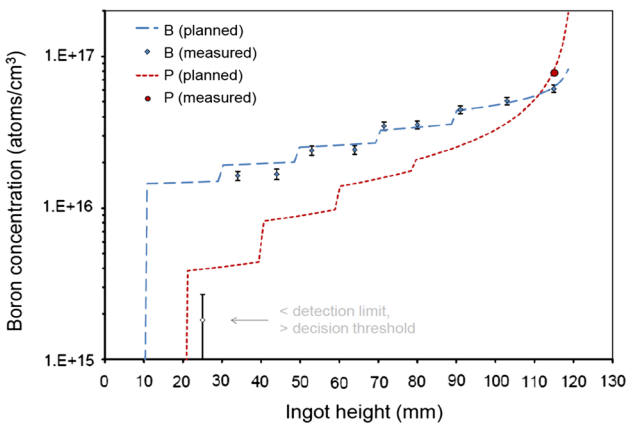

Fig. 4 Boron concentration in atoms/cm^3 in the "zebra" ingot (vertical cut). The first marked value is below the detection limit (2.2×10^{15}), but over the decision threshold (1.7×10^{15})

process at the ISE. In combination with the phosphorous measurements described in [5], it was possible detecting both dopants using non-destructive activation analysis techniques.

Influence of the crucible

Another block—p-type of the size 422 × 422 × 220 mm^3—was cut horizontally to investigate the influence of boron from the crucible material. We analyzed the influence with the following criterion of conformity from [23]:

$$\zeta = \frac{|x_1 - x_2|}{\sqrt{u^2(x_1) + u^2(x_2)}} < C \quad (4)$$

This defines that two values x_1 and x_2 have to be considered equal if ζ is below a given value of the criterion C. We chose the same intervals for decision as described in [24] (where it is used to compare a measurement to a reference value): $\zeta \leq 1.64$ (equal), $1.64 < \zeta \leq 1.95$ (probably equal), $1.95 < \zeta \leq 2.58$ (not clear), $2.58 < \zeta \leq 3.29$ (probably not equal) and $\zeta > 3.29$ (not equal). The highest boron mass fraction of $(45 \pm 6_{stat} \pm 4_{syst})$ ng/g was observed at the outer edge of the ingot and is probably not equal to the lowest value of $(22 \pm 5_{stat} \pm 3_{syst})$ ng/g found in the inner part of the ingot. The calculation was performed using only the statistical uncertainties (index "stat") which are derived from the Poisson statistics of the number of counts in the full-energy peak (netto peak area) and the baseline (mainly Compton background). The systematic error (index "syst") was not included in this calculation. It contains factors whose values are identical for the whole dataset (counting efficiency, partial gamma-ray production cross section) and thus in a comparison it cancels. We assume that there is a weak impact of the crucible on the ingot's boron mass fraction profile. The used crucible material was v-SiO_2 (vitreous, sintered, amorphous) in combination with a layer of Si_3N_4. In samples of v-SiO_2 material boron mass fractions in the range of 0.38 ± 0.2 to 0.63 ± 0.3 µg/g were found. For Si_3N_4 powder 1.83 ± 0.09 µg/g was determined.

The boron content in the crucibles and in their coating materials varied in a wide mass fraction range. Crucibles based on Si_3N_4 showed much higher boron mass fractions than the v-SiO_2 sample mentioned above—in these samples the mass fraction of boron ranges from 11.7 ± 0.6 to 17.3 ± 2.1 ng/g. In three c-SiO_2 (crystalline) samples we found boron mass fractions from 215 ± 12 to 225 ± 12 ng/g. The time required for the boron measurement depends on the size of the sample, the mass fraction, etc. A common crucible sample (mass of a few grams) with a boron mass fraction of one µg/g or more can be measured within half an hour. Taking the straightforward sample preparation of the crucibles (just dissipating bigger shards into smaller pieces) into account, it can be regarded as a fast analysis for these materials.

Results of the hydrogen analysis

Various granulates, which were made with the *fluidized bed reactor method* (FBR), were also measured with PGAA. Two aliquots (m = 2 g) for each lot ("granulate A", "granulate B") were analyzed with PGAA and combined to a weighted arithmetic mean value. The values are in a good agreement. That indicates that the lots can be regarded as homogenous. Nevertheless, the mean background corrected mass fraction of the analyzed granulates was significantly lower than the manufacturer specification based on secondary ion mass spectrometry (SIMS) measurements, see Table 1.

Distribution of hydrogen in the grains

In comparison to SIMS which determines hydrogen in a few µm near the surface, PGAA provides bulk results. The discrepancy found may be caused by an enrichment of hydrogen in the layers near the surface of the grains. If so, a cleaning procedure to remove the outer layers by grinding or etching would be conceivable. If this were the case and in the inner parts contained only minor amounts of hydrogen, the average bulk mass fraction would change with the radius r, $\sim 1/\Delta r$ for spherical geometry. Three different fractions (I—III) of granulate A were sieved and measured separately with PGAA. The results are shown in Table 1. The mass fractions of the first and the third fraction should show the clearest difference, but they are equal according to the criterion of conformity (Eq. 4) (calculated with statistical uncertainties), which means that there is no dependence on the grain radius. Although, other different distributions are also possible, the most obvious explanation to bring the PGAA and SIMS values into accordance is a local surface "contamination" with a negligible contribution to the bulk mass fraction. Nevertheless, the bulk mass fraction is the most important information for the feedstock which can be measured directly with PGAA.

Cl/H ratio

Finally, the assumption of a relation between the hydrogen and the chlorine mass fraction due to the presence of trichlorosilane gas ($SiHCl_3$) as the main precursor in the FBR process with a Cl/H mass ratio of 105.5 was checked. The same material of the two feedstock materials granulate

Table 1 Measured hydrogen mass fractions of FBR feedstock in comparison with the manufacturer's specification obtained with SIMS

Sample identifier	c_H (PGAA) (μg/g)	c_H (SIMS) (μg/g)
Granulate A		
Granulate A—aliquot 1	14.8 ± 1.0	~ 100
Granulate A—aliquot 2	15.5 ± 1.0	~ 100
Mean value	15.1 ± 0.7	~ 100
Fraction-I (3.45 ± 0.05) mm	$16.1 \pm 0.6_{stat} \pm 0.8_{syst}$	–
Fraction-II (2.67 ± 0.04) mm	$13.8 \pm 0.5_{stat} \pm 0.7_{syst}$	–
Fraction-III (2.05 ± 0.03) mm	$15.1 \pm 0.5_{stat} \pm 0.8_{syst}$	–
Granulate B		
Granulate B—aliquot 1	11.0 ± 0.9	~ 50
Granulate B—aliquot 2	11.1 ± 0.8	~ 50
Mean value	11.0 ± 0.6	~ 50

For each fraction of the lot "granulate A" the diameter and the standard deviation of the mean value is specified

A and B (see Table 1), which were analyzed with PGAA at MLZ, were also analyzed with INAA at the TRIGA Mark II research reactor of the JGU Mainz. Each sample was irradiated for 5 min at a thermal neutron flux of $\Phi_{th} = 1.7 \times 10^{12}$ cm^{-2} s^{-1} and measured after a cooling time to let interfering elements decay away. Due to the sample-to-detector distance of ~ 1.5 cm, the peak areas of the two strongest gamma lines (1642 and 2168 keV) had been corrected for summing effects. The chlorine mass fractions were found to be below the detection limit of 0.08 μg/g, thus a direct correlation between the Cl/H ratio in the samples from trichlorosilane could be excluded. An indirect hydrogen analysis by measuring the chlorine as a representative element is therefore not possible.

Conclusion and outlook

In this study, we analyzed different raw materials, parts of the crucibles, and ingots of mc-Si using PGAA. This method proves to be appropriate to analyze boron and hydrogen in these materials. The bulk analysis of hydrogen in feedstock without any chemical preparation and with a detection limit in the low μg/g region is unique. Additional NAA measurements of the FBR raw material showed that the chlorine content is much lower than expected—therefore it is not possible to use chlorine as an indicator for the hydrogen mass fraction. We found that the boron distribution in the mc-Si based p-type ingots can be described well with the Scheil equation. There is probably a weak contamination effect caused by the intake of boron from the crucible to the outer part of the ingot. For the crucibles, PGAA provides a fast analysis, if the mass fraction is in the μg/g range. The detection limits for boron in silicon reached 17 ng/g and for hydrogen in silicon 1 μg/g. Detecting even lower boron mass fractions may be possible with neutron depth profiling (NDP) or similar techniques in the future. This would be of interest for n-type ingots. At MLZ an advanced NDP environment is under construction as a supplement for the classic PGAA setup.

Acknowledgements The authors thank the Deutsche Forschungsgemeinschaft (DFG) for the funding of the project (DFG numbers HA 5471/4-1 and BO 3498/1) and the Forschungs-Neutronenquelle Heinz Maier-Leibnitz for beam time and technical support.

References

1. Arnberg L, Di Sabatino M, Øvrelid EJ (2012) State-of-the-art growth of silicon for PV applications. J Cryst Growth 360:56–60
2. Zbib MB, Norton MG, Bahr DF (2012) Effect of solute hydrogen on toughness of feedstock polycrystalline silicon for solar cell applications. Scr Mater 67(9):756–759
3. Karches B, Schön J, Gerstenberg H, Hampel G, Krenckel P, Plonka C, Ponsard B, Riepe S, Stieghorst C, Wiehl N (2017) Determination of impurity distributions in ingots of solar grade silicon by neutron activation analysis. Radiochim Acta 105(7):569–576
4. Karches B (2016) Charakterisierung von multikristallinem Solarsilicium mittels Anwendungen der Neutronenaktivierungsanalyse. PhD Thesis, Universitätsbibliothek Mainz, Mainz
5. Schön J, Schindler F, Kwapil W, Knörlein M, Krenckel P, Riepe S, Warta W, Schubert MC (2015) Identification of the most relevant metal impurities in mc n-type silicon for solar cells. Sol Energy Mater Sol Cells 142:107–115
6. Karches B, Welter K, Stieghorst C, Wiehl N, Reich T, Riepe S, Krenckel P, Gerstenberg H, Plonka C (2017) Instrumental determination of phosphorus in silicon for photovoltaics by β spectroscopy: a new approach. J Radioanal Nucl Chem 311(1):541–548
7. Schön J, Krenckel P, Karches B, Schindler F, Giesecke J, Stieghorst C, Wiehl N, Schubert MC, Riepe S (2016) Improving the material quality of silicon ingots by aluminum gettering during crystal growth. Phys Status Solidi RRL 10(10):721–724
8. Stieghorst C (2016) Neutronenaktivierungsanalyse in Archäometrie und Solarenergieforschung. PhD Thesis, Universitätsbibliothek Mainz, Mainz

9. Heinz Maier-Leibnitz Zentrum (2015) PGAA: prompt gamma and in-beam neutron activation analysis facility. J Large-Scale Res Facil 1:A20
10. Kudejova P, Révay Z, Kleszcz K, Genreith C, Rossbach M, Schwengner R, Zuber K (2015) High-flux PGAA for milligram-weight samples. In: EPJ Web of Conferences. 93:0800
11. Fazekas B, Molnár G, Belgya T, Dabolczi L, Simonits A (1997) Introducing HYPERMET-PC for automatic analysis of complex gamma-ray spectra. J Radioanal Nucl Chem 215(2):271–277
12. Tilley DR, Cheves CM, Godwin JL, Hale GM, Hofmann HM, Kelley JH, Sheu CG, Weller HR (2002) Energy levels of light nuclei $A = 5, 6, 7$. Nucl Phys A 708(1–2):3–163
13. Deruytter AJ, Pelfer P (1967) Precise determination of the branching ratio and Q-value of the 10B(n, α)^{7}Li reaction and of the Q-value of the ^{6}Li(n, α)3H reaction. J Nucl Eng 21(11):833–845
14. Magara M, Yonezawa C (1998) Decomposition of prompt gamma-ray spectra including the Doppler-broadened peak for boron determination. Nucl Instrum Methods Phys Res Sect A 411(1):130–136
15. Kudejová P (2005) Two new installations for non-destructive sample analysis: PIXE and PGAA. PhD thesis, Universität zu Köln, Köln
16. Szentmiklósi L, Gméling K, Zs Révay (2007) Fitting the boron peak and resolving interferences in the 450–490 keV region of PGAA spectra. J Radioanal Nucl Chem 271(2):447–453
17. Jolie J, Börner HG, Hoyler F, Robinson S, Dewey MS (1987) In: Robinson SJ, Copnell J, Jolie J, Stöhlker U, Rabbel V (eds) Proceedings of the 6th International Symposium on Capture Gamma-Ray Spectroscopy, Leuven, Belgium. IOP, London
18. Sakai Y, Yonezawa C, Magara M, Sawahata H, Ito Y (1994) Measurement and analysis of the line shape of prompt γ-rays from recoiling 7 Li produced in the 10B(n, α)^{7}Li reaction. Nucl Instrum Methods Phys Res Sect A 353(1–3):699–701
19. Kubo MK, Sakai Y (2000) A simple derivation of the formula of the Doppler broadened 478 keV gamma-ray lineshape from 7*Li and its analytical application. J Nucl Radiochem Sci 1(2):83–85
20. Yonezawa C (2004) In: Molnár GL (ed) Handbook of prompt gamma activation analysis. Springer, Boston
21. Scheil E (1942) Bemerkungen zur Schichtkristallbildung. Z Metall 34(34):70–72
22. Hull R (1999) EMIS datareviews series, no. 20: Properties of crystalline silicon. INSPEC IEE, London
23. Robouch P, Younes N, Vermaercke P (2003) In: PTB IT-10, pp 149–157
24. Wimolwattanapun W, Bunprapob S, Ho MD, Sutisna Oura Y, Ebihara M (2014) Quality assessment of INAA data for small-sized environmental reference samples. Anal Sci 30(8):787–792